Solar PV and BESS Plant-Level Voltage Control and Interactions: Experiments and Analysis

Lingling Fan, *Fellow, IEEE*, Zhixin Miao, *Senior Member, IEEE*, Shahil Shah, *Senior Member, IEEE*, Przemyslaw Koralewicz, *Member, IEEE*, and Vahan Gevorgian, *Senior Member, IEEE*

***Abstract*—In real world operation, low-frequency oscillations associated with plant-level voltage control of inverter-based resources (IBRs) have been a concern of grid operators. This research aims to demonstrate and analyze the effect of plant-level voltage control on system stability and potential interactions among IBRs. The experiment results of a 13.2-kV system interconnected with two IBRs —a 1-MW battery energy storage system (BESS) and a 430-kW solar photovoltaic (PV) plant —are presented. Both 0.5-Hz and 3-Hz oscillations become visible at certain conditions. The phenomenon is further explained by use of a feedback system consisting of the plant-level droop control and the effect of reactive power or var injection on voltage. The main components of the block diagram are obtained via frequency scan measurements. The analysis offers an understanding of the main contributors and other influencing factors of the 3-Hz and 0.5-Hz modes. It also reveals the role of the volt-var droop gain, the low-pass filter time constant, and the system impedance in stability.**

***Index Terms*—Inverter-based resources, plant-level control, oscillations, interactions.**

I. Introduction

PLANT-LEVEL voltage control of IBRs and the potential control interactions among IBRs have caught attention of grid operators. The NERC's inverter-based resource performance subcommittee (IRPS) reported several occasions of low-frequency oscillations possibly related with plant controls.

In 2020, South California Edison (SCE) observed several reactive power (or var) oscillation events [1]. In an event occurred in a wind plant, the plant capacity is 100 MW. The var swing can reach 65 MVAr (+28/-37) and the oscillation periodicity is about 2 minutes. These oscillations were identified by the system operator after noticing energy management system (EMS) alarms of under voltage at point of interconnection. It is also found that the the neighboring generator facility oscillated against this wind plant. The oscillation frequency is about 0.01 Hz. The plant operator found issues with the var control loop's meter, which resulted in delay of measurement data.

This material is based upon work supported by the U.S. Department of Energy's Office of Energy Efficiency and Renewable Energy (EERE) under the Solar Energy Technologies Office Award Number DE-EE0008771, and by the National Renewable Energy Laboratory, operated by Alliance for Sustainable Energy, LLC, for the U.S. Department of Energy (DOE) under Contract No. DE-AC36-08GO28308.

L. Fan and Z. Miao are with Dept. of Electrical Engineering, University of South Florida, Tampa FL 33620 (email: {linglingfan, zmiao}@usf.edu). P. Koralewicz, S. Shah, and V. Gevorgian are with the National Renewable Energy Laboratory, Golden, CO 80401 USA (e-mails: {Shahil.Shah, przemyslaw.koralewicz, vahan.gevorgian}@nrel.gov).

SCE also reported var oscillations during solar PV's active power ramping up periods. This event occurred on Dec. 30 2020. The solar plant has a capacity of 120 MW and the var swing can reach 77 MVAr (+40/-37). The oscillation periodicity is about 1 minute or 0.016 Hz. Once this oscillation was discovered, it was found that plant var output oscillated every day at start-up (sunrise). Counteracting var oscillations were observed at a local SVC and across an inter-tie line. In Tennessee, 0.29-Hz var oscillations in a solar PV plant were reported by Tennessee Valley Authority (TVA) [2]. The causations of those oscillations are under investigation.

The overall objective of this research is to demonstrate and analyze the effect of IBR's plant-level voltage control on system stability. In addition to the inverter-level control, a solar PV farm or a wind power plant usually has a plant-level control center. The plant-level control makes control decisions and sends out commands to individual solar PV inverters or wind turbines.

State-of-the-art review of droop control and its influence on stability: Frequency-power and voltage-var droop control are often employed in inverter or subsystem level [3], [4] or power plant level [5], [6] to provide frequency regulation and voltage regulation. The difference between the inverter-level implementation and plant-level implementation is whether a communication network is used. In [3], for a microgrid with PV and battery, such control is implemented at the inverter level. In the research carried out for a Scottish Phoenix project [4], reactive power to voltage droop controls are implemented at the inverter level to coordinate a 70 MVA synchronous condenser and a 70 MW battery energy storage system for reactive power sharing. In both cases, there is no communication delay for the droop control generated command signals to be processed.

On the other hand, for droop controls implemented at the plant level, communication delay has to be considered. in [7], a type-3 wind farm voltage to reactive power droop control is designed in the plant level. This control sends out commands to 23 wind turbines through a communication network to coordinate the wind turbines for reactive power injection. 150 ms delay is considered in the design evaluation process.

Prior research on wind power plant control has shown that communication delay, control gain, and the short circuit ratio (SCR) all influence system stability [7]–[9]. Specifically, [7] has shown that in the presence of large communication delays, e.g., 150 ms, a large plant-level voltage to reactive power gain can reduce the system stability margin. On the other hand, for inverter-level control where communication delays

are negligible, Vestas' experience shows that fast voltage control (or large gains) improves stability when individual wind turbines behave as stiff voltage sources [8].

While we can learn from the literature [7]–[10] to understand wind power plant's control and its effect on stability, we also would like to develop understanding on how different types of IBRs (e.g., solar PV and BESS) interact with each other in a hybrid power plant. This understanding may help us speculate the second SCE event and answer the question: Whether the nearly SVC made the oscillations worse or better?

Specifically, this research has two goals. The first goal is to develop understanding on IBR-IBR interactions through experiment design. The second goal of this research is to carry out small-signal analysis for a system with black-box components. Such analysis is enabled through a measurement-based approach.

To this end, physical experiments of a system consisting of a 1-MW BESS and a 430-kW solar PV plant have been conducted and the research results are presented this paper. Analyses were conducted to provide insights and address not only on how volt-var control and grid strength influence stability, but also how two IBRs interact.

Our contributions: In a nutshell, compared to the state-of-the-art research, e.g., wind power plant voltage control design and stability analysis (e.g., [7], [8]) which usually focuses on one plant-level voltage control and its influence, this research has a focus on a hybrid power plant's voltage control design and their effect. Such a hybrid power plant consists of IBRs of different type, e.g., solar PVs and BESS. They have different component-level characteristics as well as different communication latency. Thus our research not only examines stability of the entire system but also IBR-IBR interactions. This research also meets the needs of the grid industry. In March 2021, the power grid industry authority NERC published a reliability guide on hybrid power plants and recommended thorough studies [11].

Second, the research approach carried out in this paper can be viewed as a general approach for stability analysis of a system consisting of black-box subsystems. For such systems, we rely on measurement-based characterization to obtain frequency responses and maximumly utilize the frequency measurements for stability analysis and developing understanding on each IBR's role in oscillation modes. The analysis results match the experiment observation very well. This type of measurement-based analysis has rarely been performed on a hybrid power plant, or seen in the literature. The detailed quantitative analysis is practically useful.

The third highlight of this paper is that the research results are based on real-world BESS and solar PVs. Those measurement data presented in the paper are of reference value.

Structure of the paper: The remainder of the paper is organized as follows. Section II describes the test bed constructed at National Renewable Energy Laboratory (NREL)'s Flatirons campus. Section II also presents the hardware experiment results. Section III presents the analysis results. Section IV presents the replication study in MATLAB/Simulink. Section V concludes this paper.

II. The Test Bed and Experiment Results

The system topology is shown in Fig. 1. This entire test bed consists of 1-MW BESS and six solar PV systems with a total 430-kW capacity. The two systems are tied to the controllable grid interface (CGI) through two transformers: 400 V/13.2 kV and 600 V/13.2 kV. The volt-var droop control for the two plants are realized through SEL's real-time automatic control (RTAC) system. After many trials and errors, the test bed is able to demonstrate the var from BESS and PV oscillating again each other with a frequency at 0.5 Hz. At the meantime, the BESS var also has a 3-Hz oscillation mode. A series tests have been conducted with measurements recorded. Four consecutive cases are presented in this paper.

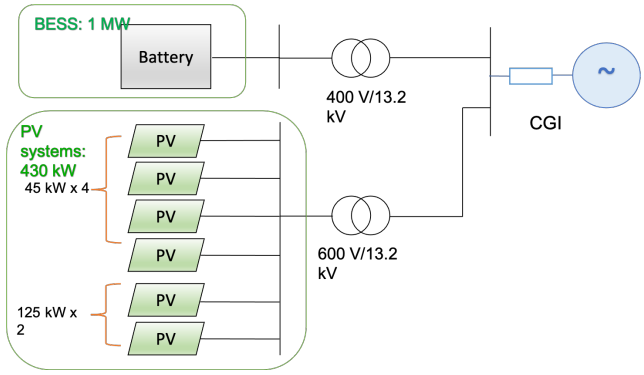

Fig. 1: The test bed setup in NREL.

Fig. 2 presents the RTAC configuration of the BESS systems. Fig. 3 presents the plant-level voltage control diagram. The voltage measurement is compared with the voltage reference and the error is passed to a low-pass filter (LPF) and amplified by a gain. The resulting var order is then sent to the inverter control. It can be seen that at steady state the gain of $\Delta Q/\Delta V = -1/\text{Droop}$. Note that the droop gain is based on per unit values of the voltage and reactive power. For solar PV and BESS, the per unit power base is different. The power base for BESS is known as 1 MW. However, for PV's power base, additional check will be made in Section III.B.

The parameters of the volt-var control and communication delay from the plant to the inverter for the two systems for the selected four cases are shown in Table I.

TABLE I: Plant-level control and delay parameters

Case	BESS			PV			X_g
	LPF	1/Droop	Delay	LPF	1/Droop	Delay	mH
12	2000	100	16	40	100	400	14.6
13	2000	200	16	40	200	400	14.6
14	2000	200	16	40	200	400	8
15	4000	200	16	40	400	400	8

*The unit of LPF and Delay time constants is ms.
*The unit of droop is p.u.

Note that 14.6 mH of the grid impedance is 0.0316 p.u. for the system of voltage base at 13.2 kV and power base at 1 MW, while 8 mH is 0.0173 p.u.. Furthermore, the droop parameters refer to voltage in p.u. to var in p.u. based on each IBR's base. For the BESS, the power base is found to be 1 MW according to the measured $\Delta Q/\Delta V$ gain at steady state, while for the solar PV, the power base is found to be 275 kW according to

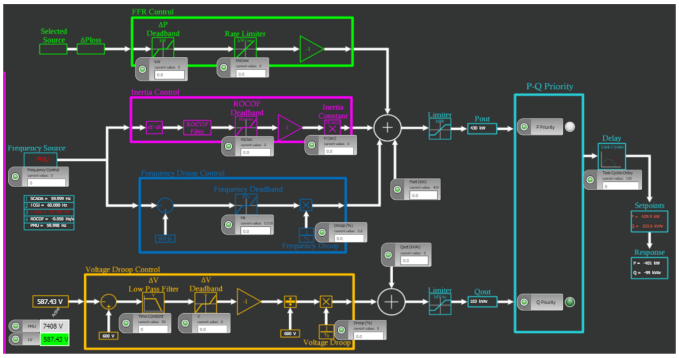

Fig. 2: RTAC setup for the BESS system. In the voltage droop control block, the measured voltage is compared with the reference value 400 V. The error is passed through a low-pass filter and modulates the var set point.

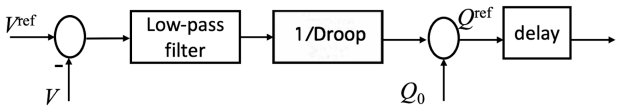

Fig. 3: The plant-level voltage control.

the measured $\Delta Q/\Delta V$ gain at steady state. Hence, even both BESS and solar PV have the same gain 100, the amounts of the var change corresponding to the same voltage drop are different. BESS will have its var increased more than three times compared to the solar PV.

A. Hardware Experiment Results

Fig. 4 presents the solar PV and BESS dynamic behavior. The dynamic event trigger is the variation in the ideal voltage source. At $t = 5$ s, the grid voltage is subject to a 1% voltage drop. At $t = 10$ s, the voltage recovers to 1 p.u. At $t = 20$ s, the grid voltage has a 1% increase. At $t = 25$ s, the voltage again recovers to 1 p.u..

For case 13, it can be clearly seen that the PV's var has a dominant mode of 0.5 Hz while the BESS's var has two dominant modes: 0.5 Hz and 3 Hz. For the 0.5-Hz mode, the BESS and the PV oscillate against each other. The voltage has both modes.

Compared to case 13, case 12 has the same settings for the grid impedance and plant-level controls, except that in case 12, both volt-var droop gains of BESS and PV are one half of that in case 13. It can be seen that the system has no visible oscillations in voltage and vars.

Compared to case 13, case 14 has the same settings for the controls except that the grid impedance is reduced from 0.04 p.u. to 0.0173 p.u.. This reduction helps the system recovers stability and there are no visible oscillations in case 14.

Case 15 has the same system impedance setting as case 14. In case 15, the LPF time constant of the BESS is doubled and the gain of the PV increases from 200 p.u. to 400 p.u. The increase in the droop gain makes 0.8-Hz oscillations visible.

Fig. 5 presents the PV and BESS var responses upon 1% voltage drop for three cases: case 12, case 14, and case 15. The steady-state change in var is to be examined. Compared to case 12, case 14 has both IBRs' control gains doubled. However, in both cases, it can be observed that the ratio of var share of BESS and PV is the same, approximately 3. This number agrees with the ratio of the two power bases: $1000/275$. For case 15, the ratio of var share reduces to 2, since the PV gain is doubled. This number also agrees with the gain ratio in a uniform power base.

III. Analysis

For analysis, we first construct a simple feedback system to represent the test bed in Fig. 1. In this feedback system, the effect of real power on the point of common coupling (PCC) voltage is ignored and only the effect of var on the PCC voltage is preserved. This assumption is reasonable since the BESS will be operating under zero real power condition. For the PV plant, the output power level is limited to 300 kW or 0.3 p.u. Given that the grid is very strong, the effect of real power on voltage can be ignored.

Fig. 6 presents a block diagram illustrating the feedback system. It can be seen that G_1 and G_2 represents the terminal voltage and var relationship of the BESS and the PV respectively. The total var injection to the PCC bus ΔQ will influence the PCC voltage:

$$\Delta V_{\text{PCC}} = \Delta V_g + X_g(\Delta Q_1 + \Delta Q_2). \tag{1}$$

Remarks: The feedback system in Fig. 6 can be used to predict stability if the real power influence is ignored. This system has a similar feature as Fig. 8 in [7] (albeit there is one IBR only) focusing on voltage and var relationship only. When the real power dispatch level is low, such omission is reasonable. On the other hand, if the effect of real power or real current influence is to be considered in the high power exporting and weak grid scenarios, this feedback system has to be updated to include the real current effect. A block diagram with real current influence considered has been presented in [12] and used to explain why 0.1-Hz oscillations appear in reactive power when solar PV power plants ramp up real power.

A. Identifying grid impedance

It can be seen that if the grid voltage stays constant, the PCC voltage is proportional to the total var injection. This relationship can help us cross validate the value of X_g. Fig. 7 presents the PCC voltage, the total var from the BESS and the PV. The dynamics are triggered by a step change in the BESS's var order. This comparison shows that though X_g is 0.0316 p.u. based on the given number of inductance, it appears that X_g at 0.04 p.u. can make the PCC voltage match better with $0.4 \times Q$, where Q is the sum of var injection from the PV and the BESS. Past experiences also indicate that the real inductance value may deviate from the value in the name plate [13]. Therefore, in the analysis follows, X_g will be assumed to be 0.4 p.u. for case 12 case 13. For case 14 and case 15, 0.0173 p.u. is a reasonable number for X_g as we can see that the PCC voltage deviation after Gauss filter matches well with $0.0173 \times Q$.

This article has been accepted for publication in IEEE Transactions on Energy Conversion. This is the author's version which has not been fully edited and content may change prior to final publication. Citation information: DOI 10.1109/TEC.2023.3237084

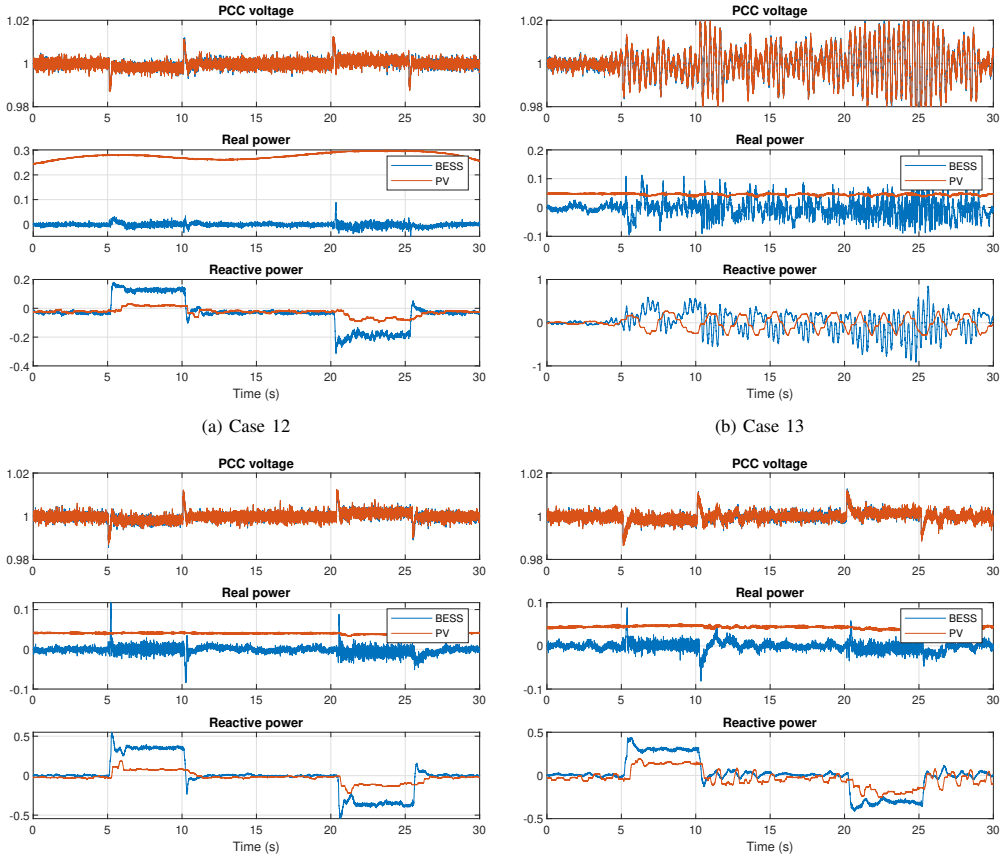

(a) Case 12 (b) Case 13

(c) Case 14 (d) Case 15

Fig. 4: Dynamic behavior of the PV and BESS systems upon a 1% voltage drop in the grid voltage.

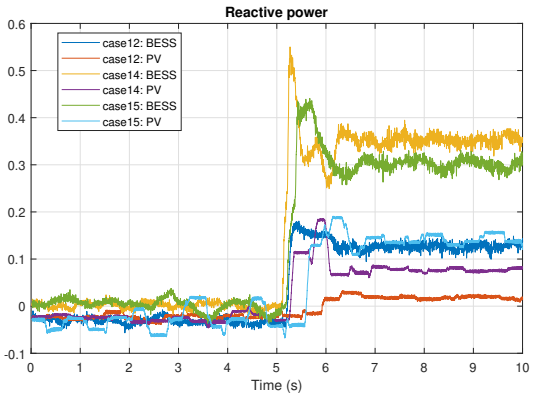

Fig. 5: Var responses from BESS and PV for three cases.

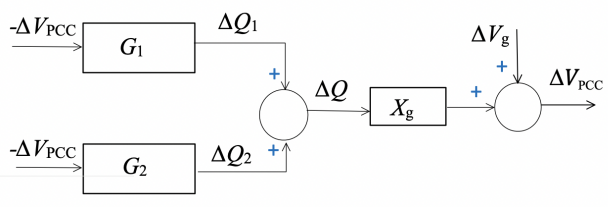

Fig. 6: The feedback system considering voltage and var relationship.

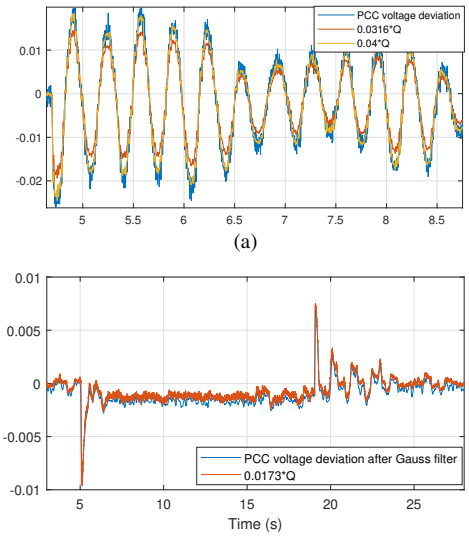

(a)

(b)

Fig. 7: (a) Comparison of the PCC voltage magnitude ΔV versus $0.0316 \times Q$ and $0.04 \times Q$ at Case 13. (b) Comparison of the PCC voltage magnitude versus $0.0173 \times Q$ at Case 15.

B. Identifying G_1 and G_2 via frequency-domain response measurements

Further experiments are designed to find G_1 and G_2. For each scenario, the CGI's voltage source's magnitude is perturbed with a sinusoidal injection at a frequency in the range

of 0.025 Hz to 40 Hz. The PCC voltage and the vars from the BESS and the PV are recorded and the Fourier transform is performed to extract the phasors at the perturbed frequency.

The details of the sensor information and the procedure of perturbation and data post-processing have been reported in [14]. Using the CGI, frequency scans have been conducted to extract dq-frame admittance in the range of 0.1-1000 Hz [15] and sequence-domain impedance in the range of 1-1000 Hz [16]. In the current research, the frequency responses of volt-var in the lower frequency range are measured since the focused dynamics have a bandwidth less than 10 Hz. The frequency responses of the vars versus the PCC voltage for case 12, case 14, and case 15 are obtained and presented in Fig. 8a and Fig. 8b.

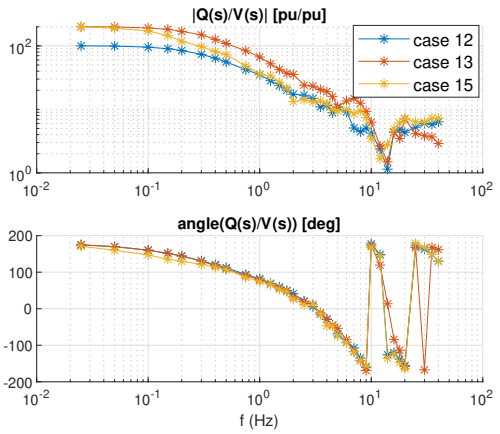

(a)

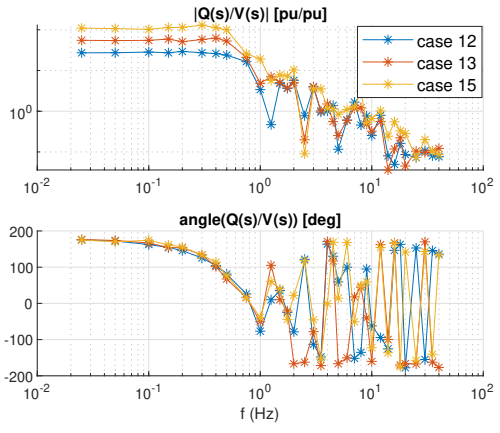

(b)

Fig. 8: V-Q frequency response measurements for BESS and PV. (a) BESS measurements of $-G_1$. (b) PV measurements of $-G_2$.

Remarks on the bases of BESS and PV: The frequency responses of $\Delta Q/\Delta V$ of the 1-MW BESS at very low frequency range implicate the steady-state gain. Fig. 8(a) shows that the BESS has a gain of 100 for case 12 and 200 for case 13 and case 15. The measured data confirm that at case 12 the gain of $\Delta Q/\Delta V$ is 100, while at case 13 and case 15, this gain is 200.

The frequency responses of $\Delta Q/\Delta V$ of the 430-kW PV plant (Fig. 8(b)) at very low frequency range indicate that the steady-state droop gain is 27.5, 55, and 110 for case 12, case 13, and case 15. These numbers do not align with the gains 100, 200 and 400 in Table I. If the PV system base is 275 kW, instead of 430 kW, then the gain $\Delta Q/\Delta V$ of 100 at the PV system base is 27.5 at the 1-MW base. Therefore, it is found that the PV system's base is 275 kW.

If the PV's base is 275 kW, then for cases 12 and 14, the var sharing ratio of BESS and PV should be $100 : 27.5$. For case 15, the ratio should be $200 : 400 \times 0.275 = 200 : 110$. We may use Fig. 5 for further confirmation. It can be seen that for case 12, the ratio of BESS vs. PV in terms of var change is $0.17 : 0.05 = 100 : 29.6$. For case 14, the ratio is $0.35 : 0.1 = 100 : 28.6$. For case 15, the ratio is $0.30 : 0.166 = 200 : 112$. It can be seen that the experiment results agree with the conjecture that the PV base is 275 kW.

Remarks on the effect of the LPF time constant: Fig. 8(a) presents the Bode diagram of $\Delta Q/\Delta V$ for BESS in three cases: case 12, case 13, and case 15. Compared to case 13, in case 12, the gain of the voltage control is reduced by half. This can also be seen in Fig. 8(a) that the magnitude in case 12 is half of that in case 13 in the interested frequency range of 0.01 Hz to 10 Hz. The angles of the gain are the same for two cases. Compared to case 13, in case 15, the LPF's time constant has been doubled. That reflects in the the Bode diagram of $\Delta Q/\Delta V$ as the magnitude in case 15 is the same as that in case 13 for the frequency range of less than 0.1 Hz, and is less compared to that in case 13 for the frequency greater than 0.1 Hz. In the 1 Hz - 5 Hz range, the gain is same as that of case 12.

In short, a LPF with a larger time constant reduces the magnitude of $\Delta Q/\Delta V$ in a certain frequency range. For the voltage-var feedback system, the LPF with a larger time constant helps reduce the loop gain and can improve the stability for the interested dynamics, i.e., the 3-Hz oscillations.

C. Time-domain step responses

In addition to the set up shown in Fig. 1, two more test beds were set up (Testbed 2 and Testbed 3), each consisting of the CGI and one IBR plant. The CGI is controlled to produce voltage step change. The responses of the IBR are recorded.

Fig. 9 presents the BESS responses upon 1% voltage step down in the ideal voltage source. Fig. 10 presents the PV responses upon 1% voltage step down in the ideal voltage source.

1) Delay: For the BESS only test bed, it can be seen that the PCC voltage immediately drops to 0.99 p.u. upon the ideal voltage source step down. From the time-domain response, the var takes about 0.1 s to start to respond to the voltage error. For the PV only test bed, case 12 results are analyzed. The voltage error and the var are plotted together to better analyze the delay effect. Fig. 11 presents the results. It can be clearly seen that the PV has a larger delay (about 0.4 s) compared to BESS (0.1 s).

The delay can also be computed from the frequency-domain response of $\Delta Q/\Delta V$ in Fig. 8. For BESS, the phase angle of $\Delta Q/\Delta V$ shows that -2π change in every 10 Hz. For PV, the phase angle shows that -2π change in about 2 Hz. The group

This article has been accepted for publication in IEEE Transactions on Energy Conversion. This is the author's version which has not been fully edited and content may change prior to final publication. Citation information: DOI 10.1109/TEC.2023.3237084

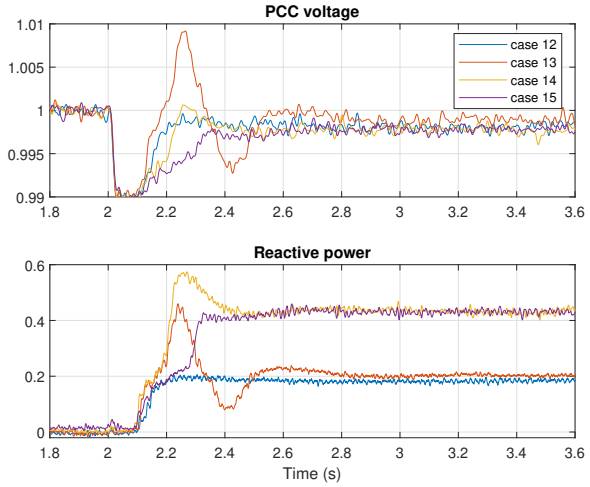

Fig. 9: Tested 2 responses when the CGI voltage is subject to 1% step down.

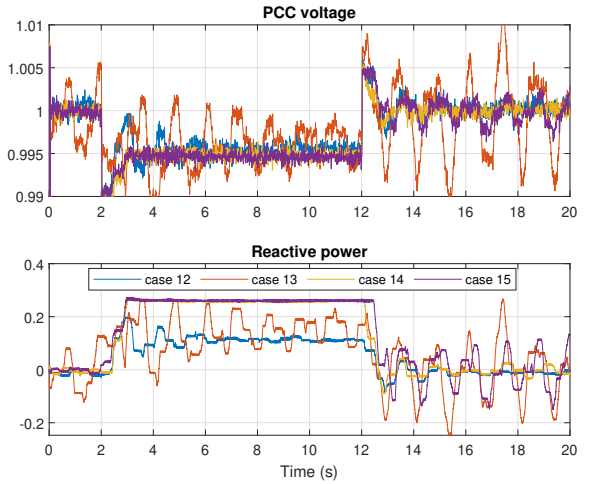

Fig. 10: Testbed 3 responses when the CGI voltage is subject to 1% step down.

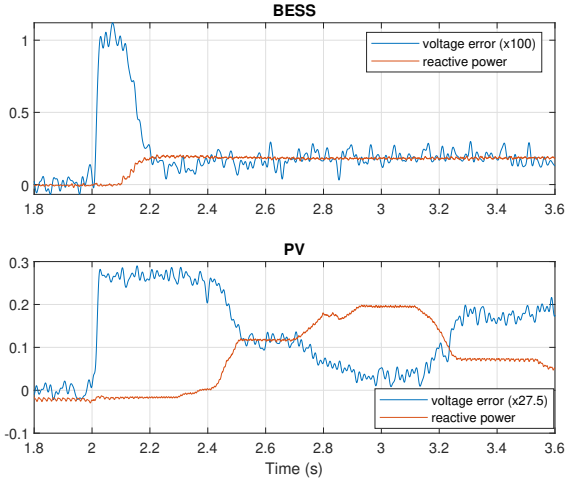

Fig. 11: Testbed 2 and Testbed 3's voltage error and var response.

delay, defined as the rate of angle change over frequency [17], is about 0.1 s.

$$\text{group delay}_{\text{BESS}} = \frac{2\pi \text{ rad}}{10 \times 2\pi \text{ rad/s}} = 0.1s.$$

The group delay can also be found for the PV as 0.5 s.

$$\text{group delay}_{\text{PV}} = \frac{2\pi \text{ rad}}{2 \times 2\pi \text{ rad/s}} = 0.5s.$$

2) Steady-state analysis: Steady-state analysis may be carried out using the block diagram in Fig. 6. It can be seen that the var and the grid voltage has the following relationship:

$$\Delta Q_{\text{BESS}} = -\frac{G_1}{1 + G_1 X_g} \Delta V_g \tag{2}$$

$$\Delta Q_{\text{PV}} = -\frac{G_2}{1 + G_2 X_g} \Delta V_g \tag{3}$$

At steady state, G_1 and G_2 are the voltage control gains. Therefore, for -0.01 change in V_g, the BESS and PV's var change can be found. Table II lists the parameters and the computed ΔQ_{BESS} and ΔQ_{PV}.

It can be seen that the var responses of the BESS in Fig. 9 agree with the analysis results. The var responses of the PV in Fig. 10 agree with the analysis results for case 12 and case 13. For case 14 and case 15, the physical system has a limit at 0.27 p.u. Thus, the var of the PV for these two cases are capped at this limit.

TABLE II: Steady-state G_1, G_2, and X_g for cases 12-15.

	G_1	G_2	X_g	ΔQ_{BESS}	ΔQ_{PV}
case 12	100	27.5	0.04	0.20	0.13
case 13	200	55	0.04	0.22	0.17
case 14	200	55	0.0173	0.45	0.28
case 15	200	110	0.0173	0.45	0.28

It can also be found from Fig. 10 that that the PV only system has poorly damped oscillations for case 13 and case 15. The oscillations are visible in both the PCC voltage and the var after 12 s when the ideal voltage source recovers to 1 p.u.

D. Stability analysis

Based on the block diagram presented in Fig. 6, if the voltage feedback to both PV and BESS is decoupled, the loop gain can be found as:

$$\text{Loop Gain} = \left(G_1(s) + G_2(s)\right) X_g. \tag{4}$$

For case 12 and case 13, $X_g = 0.04$ p.u. For case 15, $X_g = 0.0173$ p.u. $G_1(s)$ and $G_2(s)$ are all different for the three cases, as shown in Fig. 8.

If the system has only PV integrated, the loop gain becomes the following:

$$\text{Loop Gain} = G_2(s) X_g. \tag{5}$$

There are multiple loop gains depending on how we decouple the system. The loop gains can be found If only the voltage feedback to the PV (or the BESS) is decoupled:

$$\text{PV: : Loop Gain 1} = \frac{\Delta Q_2}{\Delta Q} = G_2(s) \frac{X_g}{1 + X_g G_1(s)}, \tag{6}$$

$$\text{BESS: : Loop Gain 2} = \frac{\Delta Q_1}{\Delta Q} = G_1(s) \frac{X_g}{1 + X_g G_2(s)}. \tag{7}$$

Fig. 12 presents the Bode plots of the loop gains of (4) for three cases. From Fig. 12(a) It can be seen that case 13 is

marginally stable, while the other two cases are stable. At 3 Hz, all three cases show phase crossover. Both case 12 and case 15 have their gains below 0 dB. On the other hand, case 13 has a gain at 0 dB. This analysis result aligns with the observed experiment results that case 13 has most severe oscillations.

Since this loop gain mainly focuses on the PCC voltage, we may examine the other loop gain in Fig. 12(b), which focuses on PV's var. Fig. 12(b) shows that for case 13, there are two peaks, one at 0.5 Hz and the other at 3 Hz. The loop gain has a phase crossover frequency at about 0.8 Hz for all three cases. Case 15 has the least phase margin. This implicates that the PV var should expect to see 0.8-Hz oscillations in case 15. This observation corroborates the experiment results in Fig. 4.

Fig. 12(c) shows Loop Gain 2, when the voltage feedback to the BESS is decoupled. Loop Gain 2 shows that at 3 Hz, phase crossover happens for all three cases. The gain margin of case 13 is 0, indicating marginal instability of case 13. The frequency response of Loop Gain 2 shows that for all three cases, the magnitude shows a peak at 0.8 Hz. Case 13 has the largest magnitude. This implicates that the var of BESS should show both 0.5-0.8 Hz and 3 Hz oscillations.

1) Main influencer of 3-Hz and 0.5-Hz modes: Additional analysis is carried out to examine which one, BESS or PV, plays a major role in causing the 3-Hz and 0.5-Hz oscillations.

When the system has only PV integrated, it is found from the Bode plots of the loop gain (shown in Fig. 13) that while case 12 shows adequate phase margin at 0.5 Hz and gain margin at 0.8 Hz, the other two cases do not appear to have adequate phase margin and gain margin. Therefore, it is expected that the system may show ~ 0.8-Hz oscillations for case 13 and case 15. Fig. 13 indicates that the PV is the major influencer of the 0.5-Hz mode.

The frequency responses of BESS and PV are plotted together for case 13 and shown in Fig. 14.

It can be clearly see that the loop gain is mainly influenced by BESS' frequency response. Therefore, it can be concluded that BESS contributes to the 3-Hz oscillation mode. At 3 Hz, G_1 has a much larger magnitude than G_2. This explains why 3-Hz oscillations are visible in BESS var, but not visible in the PV's var for case 13.

2) Interactions: The phase angles of G_1 and G_2 at 3 Hz are $-180°$ and $-100°$. If we view G_1 and G_2 as two parallel admittances, then both have negative conductance. That is, while the BESS is the main contributor of the 3-Hz oscillation mode, PV makes the 3-Hz oscillations worse.

For 0.5-Hz mode, the two do not behave similarly. It can be seen in the range of 0.5 Hz and 1 Hz, while G_1 (BESS) has an angle in the range of $-45°$——$-90°$, G_2 (PV) has an angle in the range of $-120°$——$-180°$. That is, while the PV contributes a negative conductance at 0.5 Hz, BESS counters a positive conductance. In another word, while PV is the major contributor of the 0.5-Hz mode, BESS helps provide damping of the oscillations. The large phase angle difference also explains why the PV and the BESS appear oscillating again each at 0.5 Hz in case 13 and at 0.8 Hz in case 15.

Remarks: Based on the frequency-domain analysis, it is found that the BESS contributes to the 3-Hz oscillation mode while the PV contributes to the 0.5-Hz oscillation mode. In addition, PV makes the 3-Hz mode worse while the BESS makes the 0.5-Hz mode better. The analysis results corroborate the experiment results.

When there is only BESS, the system has a well-damped 3-Hz mode for case 13. When there is only PV, both case 13 and case 15 show unstable 0.5-Hz oscillations. When there are

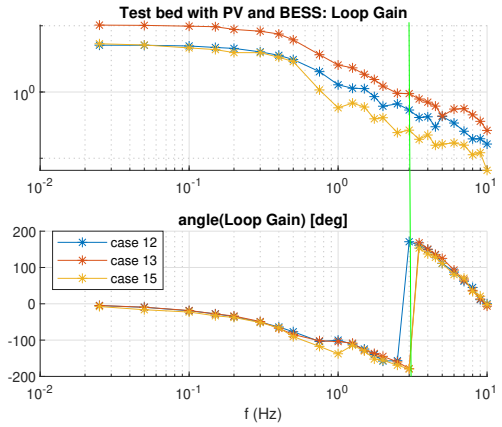

(a)

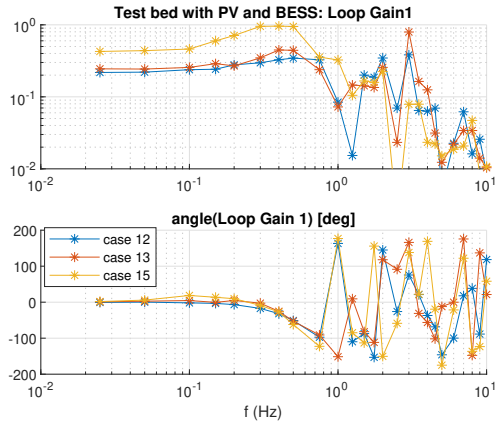

(b)

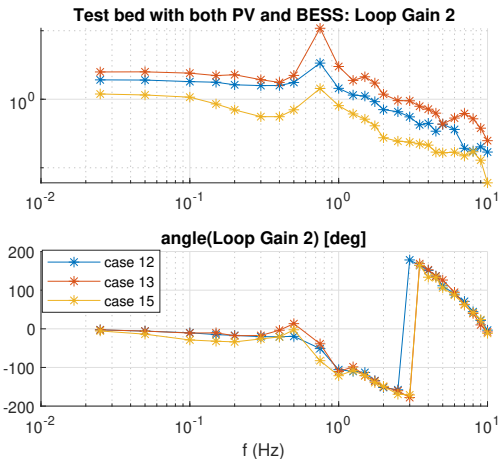

(c)

Fig. 12: (a) Loop gain when the voltage feedback to both the PV and BESS is decoupled. (b) Loop gain 1 when the voltage feedback to the PV is decoupled. (c) Loop gain 2 when the voltage feedback to the BESS is decoupled.

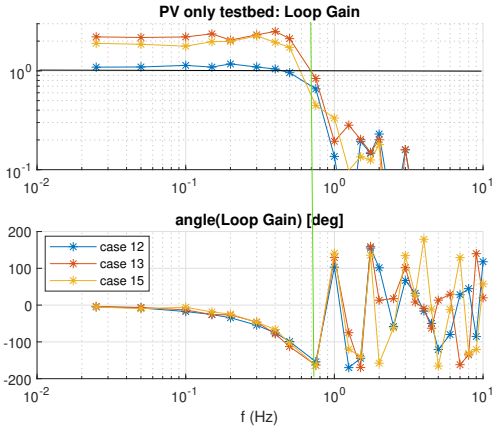

Fig. 13: Loop gains when only PV is integrated.

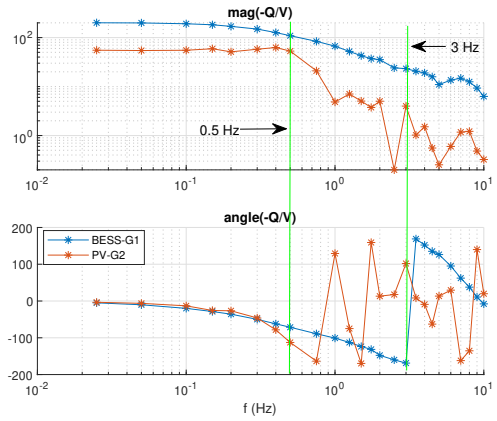

Fig. 14: Frequency responses of BESS G_1, PV G_2 for case 13.

both BESS and PV, for case 13, both the 3-Hz mode and the 0.5-Hz mode appear.

The large voltage to var gain and the system impedance have the similar effect to increase the loop gain, driving the system to instability. On the other hand, a larger time constant in the low-pass filter of BESS implicates a reduced gain at frequencies above 1 Hz. Thus, case 15 does not have stability issue.

The interaction analysis can help relate the real-world observation of an SCE event when a solar PV oscillated against an SVC in var. Based on the above analysis, it can be reasoned that the solar PV and SVC have a large phase angle difference in their $\Delta Q/\Delta V$ response at the oscillation frequency. Furthermore, the SVC helps contributing damping to the oscillations.

Remarks: Through this research, it can be seen that plant-level voltage control design needs to consider subsystems' characteristics. The first rule is to avoid a large loop gain. Weak grid or a large grid impedance, and the plant-level large voltage control gain can all contribute to a large loop gain. Therefore, a large voltage control gain is to be used with caution. Should a large gain has to be used, a low-pass filter with suitable time constant can help keep the gain the same at the steady-state, but with a reduced value in the higher frequency range. This can help improve stability margin.

IV. Replication Study

Finally, in the last section, a replication study is presented by constructing a feedback system shown in Fig. 6. The objective of the replication study is to examine whether such a modeling assumption makes sense. The replication study will demonstrate how the PV and the BESS behave when they are interconnected together given that their frequency responses are similar as those obtained from the measurement. If the simulation study shows that their behavior is similar as that observed in the hardware experiments, then the modeling assumption we use in this paper is sound.

Both G_1 and G_2 are are explicitly modeled. Both consist of a delay unit and one or two low-pass filters. The transfer functions are tuned to create the desired frequency responses.

$$G_1(s) = K_1 e^{-0.075s} \frac{1}{(t_{\text{BESS}}s+1)(0.01s+1)}$$

$$G_2(s) = K_2 e^{-0.3s} \frac{1}{(0.0714s^2+0.2857s+1.0)(0.01s+1)}$$

where K_1 and K_2 are voltage control gains, t_{BESS} is 0.425 s for cases 12-14, and 0.425×2 s for case 15. The resulting frequency-domain responses are shown in Fig. 15. The frequency responses can approximate the BESS and the PV responses.

A feedback system was constructed in MATLAB/Simulink, shown in Fig. 16. Simulation results for the three test beds are shown in Figs. 17 and 18. Specifically, Testbed 2 (BESS only) shows well damped 3-Hz oscillations for case 13 while Testbed 3 (PV only) shows undamped 0.5-Hz oscillations for case 13 and case 15. When both BESS and PV are included in Testbed 1, the system is very stable for case 12 and case 14. For case 15, 0.8-Hz oscillations are observed. For case 13, 3-Hz oscillations are dominant while 0.5-Hz oscillations are also visible in var.

The linear feedback system models are capable of replicating a few critical features of the studied system.

- BESS is the contributor of the 3-Hz oscillations. PV makes the 3-Hz mode worse.
- PV is the contributor the 0.5-Hz oscillations. BESS makes the 0.5-Hz mode better.
- The voltage control gains and the system impedance have the similar effect. Increasing the gains and the impedance drive the system to instability.

V. Conclusion

This paper presents a systematic approach to understand the effect of plant-level control on dynamic stability of a hybrid power plant consisting of a 430-kW PV and 1-MW BESS. The IBRs are black boxes and have limited information available for model construction. The main contributions of this paper include (i) the development of a feedback block diagram suitable for stability analysis, (ii) identification of the subsystem models via frequency-domain responses and time-domain data, and (iii) identification of the main influencers of oscillation modes and the intricate interactions played by IBRs on each mode.

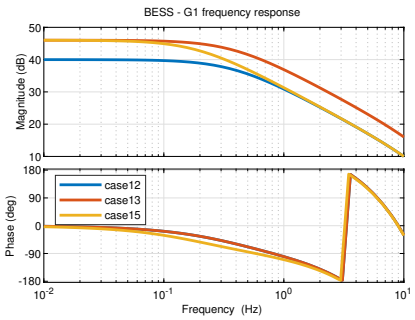

(a)

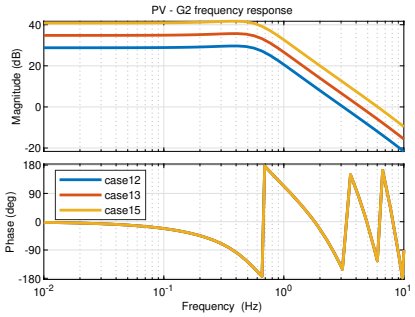

(b)

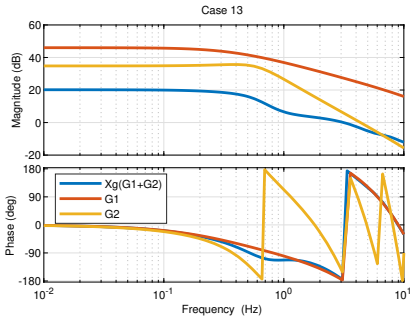

(c)

Fig. 15: Frequency responses. (a) BESS G_1 for cases 12, 13, and 15, (b) PV G_2 for cases 12, 13, and 15, and (c) the loop gain $(G_1 + G_2)X_g$ for case 13.

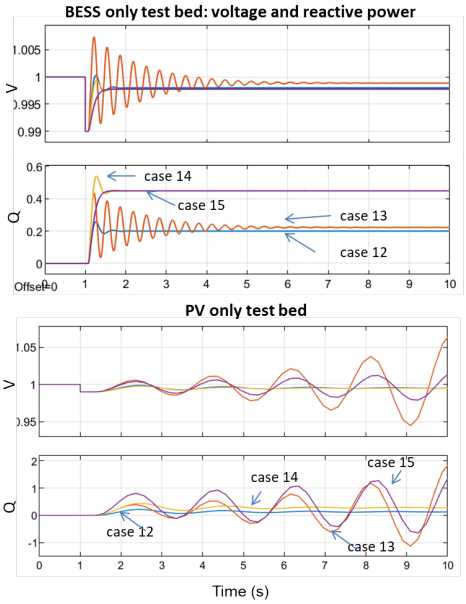

Fig. 17: Simulation results of Test bed 2 and Test bed 3 upon 1% voltage drop in V_g.

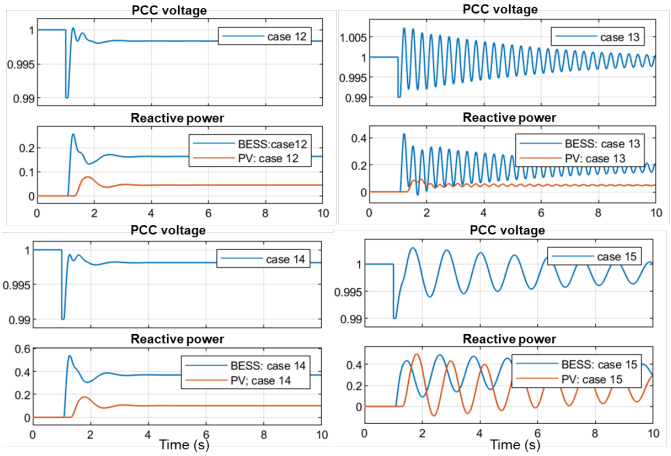

Fig. 18: Simulation results of Test bed 1 upon 1% voltage drop in V_g.

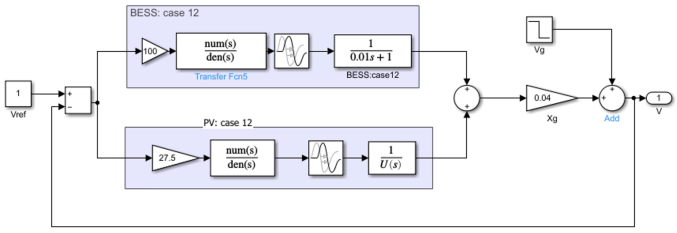

Fig. 16: Simulink model for Testbed 1.

ACKNOWLEDGEMENT

The authors would like to thank the anonymous reviewers and editor for suggestions to improve this paper.

REFERENCES

[1] D. Piper. (2021) Forced Oscillations in Renewable Generation MVAR. [Online]. Available: https://www.nerc.com/comm/RSTC/IRPWG/IRPWG_Jan_20_2021_Meeting_Presentations.pdf

[2] G. Kobet. (2021) IBR Oscillations in TVA. [Online]. Available: https://www.nerc.com/comm/RSTC/IRPWG/IRPWG_Meeting_Presentations_-_2021_08_19.pdf

[3] H. Mahmood, D. Michaelson, and J. Jiang, "A power management strategy for pv/battery hybrid systems in islanded microgrids," *IEEE Journal of Emerging and Selected Topics in Power Electronics*, vol. 2, no. 4, pp. 870–882, 2014.

[4] M. Nuhic and G. Yang, "A hybrid system consisting of synchronous condenser and battery-enhanced services for weak systems," in *2019 IEEE PES Innovative Smart Grid Technologies Europe (ISGT-Europe)*. IEEE, 2019, pp. 1–5.

[5] Y. Zhou, Y. Zhan, Q. Yu, D. Guru, and P. Zhao, "Electrical pre-design for grid code compliant evaluation of wind power plant in vestas," in *2011 Asia-Pacific Power and Energy Engineering Conference*. IEEE, 2011, pp. 1–7.

[6] J. Van de Vyver, J. D. De Kooning, B. Meersman, L. Vandevelde, and T. L. Vandoorn, "Droop control as an alternative inertial response strategy for the synthetic inertia on wind turbines," *IEEE Transactions on Power Systems*, vol. 31, no. 2, pp. 1129–1138, 2015.

[7] J. Martínez, P. C. Kjær, P. Rodriguez, and R. Teodorescu, "Design and analysis of a slope voltage control for a dfig wind power plant," *IEEE Transactions on Energy Conversion*, vol. 27, no. 1, pp. 11–20, 2012.

[8] Y. Zhou, D. D. Nguyen, P. C. Kjær, and S. Saylors, "Connecting wind power plant with weak grid - challenges and solutions," in *2013 IEEE Power & Energy Society General Meeting*, 2013, pp. 1–7.
[9] J. Martínez, P. C. Kjær, P. Rodriguez, and R. Teodorescu, "Comparison of two voltage control strategies for a wind power plant," in *2011 IEEE/PES Power Systems Conference and Exposition*, 2011, pp. 1–9.
[10] J. Kim, J.-K. Seok, E. Muljadi, and Y. C. Kang, "Adaptive q–v scheme for the voltage control of a dfig-based wind power plant," *IEEE Transactions on Power Electronics*, vol. 31, no. 5, pp. 3586–3599, 2016.
[11] NERC. (2021, March) Reliability Guideline: Performance, Modeling, and Simulations of BPS connected Battery Energy Storage Systems and Hybrid Power Plants.
[12] L. Fan, Z. Miao, D. Piper, D. Ramasubramanian, L. Zhu, and P. Mitra, "Analysis of 0.1-hz var oscillations in solar photovoltaic power plants," *IEEE Transactions on Sustainable Energy*, 2022.
[13] L. Bao, L. Fan, Z. Miao, and Z. Wang, "Hardware demonstration of weak grid oscillations in grid-following converters," in *2021 North American Power Symposium (NAPS)*, 2021, pp. 01–06.
[14] L. Fan, Z. Miao, S. Shah, P. Koralewicz, V. Gevorgian, and J. Fu, "Data-driven dynamic modeling in power systems: A fresh look on inverter-based resource modeling," *IEEE Power and Energy Magazine*, vol. 20, no. 3, pp. 64–76, 2022.
[15] L. Fan, Z. Miao, P. Koralewicz, S. Shah, and V. Gevorgian, "Identifying DQ-domain admittance models of a 2.3-MVA commercial grid-following inverter via frequency-domain and time-domain data," *IEEE Transactions on Energy Conversion*, vol. 36, no. 3, pp. 2463–2472, 2021.
[16] S. Shah, P. Koralewicz, V. Gevorgian, and R. Wallen, "Sequence impedance measurement of utility-scale wind turbines and inverters – reference frame, frequency coupling, and MIMO/SISO forms," *IEEE Transactions on Energy Conversion*, vol. 37, no. 1, pp. 75–86, 2022.
[17] A. V. Oppenheim, *Discrete-time signal processing*. Pearson Education, 1999.

Lingling Fan (Fellow, IEEE) received the B.S. and M.S. degrees in electrical engineering from Southeast University, Nanjing, China, in 1994 and 1997, respectively, and the Ph.D. degree in electrical engineering from West Virginia University, Morgantown, in 2001. Currently, she is Professor at the University of South Florida, Tampa, where she has been since 2009. She was a Senior Engineer in the Transmission Asset Management Department, Midwest ISO, St. Paul, MN, form 2001 to 2007, and an Assistant Professor with North Dakota State University, Fargo, from 2007 to 2009. Her research interests include power systems and power electronics. Dr. Fan serves as Editor-in-Chief for IEEE Electrification Magazine and Associate Editor for IEEE Trans. Energy Conversion.

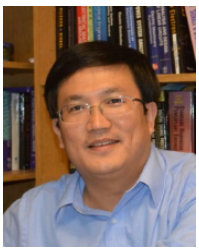

Zhixin Miao (Senior Member, IEEE) received the B.S.E.E. degree from the Huazhong University of Science and Technology,Wuhan, China, in 1992, the M.S.E.E. degree from the Graduate School, Nanjing Automation Research Institute (Nanjing, China) in 1997, and the Ph.D. degree in electrical engineering from West Virginia University, Morgantown, in 2002.

Currently, he is with the University of South Florida (USF), Tampa. Prior to joining USF in 2009, he was with the Transmission Asset Management Department with Midwest ISO, St. Paul, MN, from 2002 to 2009. His research interests include power system stability, microgrids, and renewable energy. Dr. Miao serves as Associate Editor for IEEE trans. Sustainable Energy.

Shahil Shah (Senior Member, IEEE) received the B.E. degree from Government Engineering College, Gandhinagar, India, in 2006, the M.Tech. degree from the Indian Institute of Technology (IIT) Kanpur, Kanpur, India, in 2008, and the Ph.D. degree from Rensselaer Polytechnic Institute (RPI), Troy, NY, in 2018, all in electrical engineering.

Before joining the Ph.D. program, he worked in India at Bhabha Atomic Research Center, Siemens Corporate Technology, and GE Global Research. He is currently a senior engineer for grid integration in the National Renewable Energy Laboratory (NREL), Golden, CO. His research focusses on dynamic and transient stability of renewable energy systems and power systems with high levels of inverter-based resources. He is serving as an associate editor of the IEEE Transactions on Energy Conversion.

Przemyslaw Koralewicz (Member, IEEE) received the M.S.E.E. degree from Silesian Technical University, Gliwice, Poland, in 2010. He specializes in modeling, detailed analysis, and testing of smart inverters and complex power systems including microgrids. He is utilizing the National Renewable Energy Laboratory Controllable Grid Interface, a new, groundbreaking testing apparatus and methodology to test and demonstrate many existing and future advanced controls for various renewable generation technologies on the multi-megawatt scale and medium-voltage levels.

Vahan Gevorgian (Senior Member, IEEE) received the Ph.D. degree in electrical engineering from the State Engineering University of Armenia, Yerevan, Armenia, in 1993. He joined National Renewable Energy Laboratory (NREL) in October 1994 and has served many roles over the years. He is currently working with the Power Systems Engineering Center focused on renewable energy impacts on transmission and interconnection issues and dynamic modeling of variable generation systems. He research interests include dynamometer and field testing of large and small wind turbines, dynamometer testing of wind turbine drivetrain components, development of advanced data acquisition systems, and wind turbine power quality. He provides technical support to NREL industry partners and major U.S. wind turbine manufacturers. He is member of the IEC Team for wind turbine power quality standards. His contributions to NREL research have been recognized through multiple Outstanding Individual and Team Staff awards.